Seasonal and QBO variations of ascent rate in the tropical lower stratosphere as inferred from UARS HALOE trace gas data

Masanori Niwano
Department of Geophysics, Kyoto University, Kyoto, Japan

Koji Yamazaki
Graduate School of Environmental Earth Science, Hokkaido University, Sapporo, Japan

Masato Shiotani
Radio Science Center for Space and Atmosphere, Kyoto University, Kyoto, Japan

Received 17 June 2003; revised 22 September 2003; accepted 9 October 2003; published 27 December 2003.

[1] Seasonal and interannual variations in ascent rates are investigated as a function of latitude and height, using water vapor (H_2O) and methane (CH_4) data from the stratospheric measurements of the Halogen Occultation Experiment (HALOE). The ascent rate is inferred from the ascending signal of variations in the entry value of $[H_2O] + 2[CH_4]$ ($\hat{H}$). Within ±15° of the equator the derived ascent rate exhibits two kinds of dominant variations with a clear latitudinal structure, seasonal variation, and the quasi-biennial oscillation (QBO). The seasonal cycle exhibits a vertically in-phase variation, with a northern winter maximum of 0.2–0.4 mm s^{-1} and a summer minimum of ~0.2 mm s^{-1} in the 20–60 hPa layer. The latitudinal structure is characterized by an early appearance of a subtropical summer maximum of the ascent rate and by double peaks at 10–15°N and S during the northern winter season. The QBO component of the ascent rate shows tropically confined anomalies with a rapid downward propagation, but mass attenuation anomalies estimated from the ascent rate show a much slower downward propagation. The descent anomalies exhibit a well-structured and equatorially symmetric variation, while the ascent anomalies have a tendency to propagate latitudinally. This might be connected with the phase dependency of the QBO acceleration. An examination of the phase and amplitude of the ascent rate and temperature for both the seasonal and QBO components emphasizes that the radiative damping timescale is considerably long (40–100 days) below 40 hPa. *INDEX TERMS:* 0341 Atmospheric Composition and Structure: Middle atmosphere—constituent transport and chemistry (3334); 3334 Meteorology and Atmospheric Dynamics: Middle atmosphere dynamics (0341, 0342); 3319 Meteorology and Atmospheric Dynamics: General circulation; *KEYWORDS:* mean meridional circulation, transport, water vapor

Citation: Niwano, M., K. Yamazaki, and M. Shiotani, Seasonal and QBO variations of ascent rate in the tropical lower stratosphere as inferred from UARS HALOE trace gas data, *J. Geophys. Res.*, *108*(D24), 4794, doi:10.1029/2003JD003871, 2003.

1. Introduction

[2] Mean meridional circulation in the tropical lower stratosphere has an important role in determining the stratospheric transport of air of tropospheric origin. Air mass is distributed to the whole middle atmosphere by tropical upwelling and extratropical poleward flow in the lower stratosphere, and by meridional flow from the summer to the winter hemisphere in the upper stratosphere and the mesosphere [e.g., *Dunkerton*, 1978]. The mean meridional circulation in the middle atmosphere is produced by planetary waves, synoptic waves, and gravity waves, as illustrated in *Plumb* [2002]. Additional tropical thermal forcing is also necessary to drive the observed upwelling maximum on the summer side of the lower stratosphere [*Plumb and Eluszkiewicz*, 1999; *Semeniuk and Shepherd*, 2001]. In the lower stratosphere, longwave heating by ozone absorption of upward radiative flux from the troposphere could deform tropical upwelling [*Norton*, 2001].

[3] The stratospheric meridional circulation in the tropics is mainly modulated by two dominant kinds of variations: seasonal and quasi-biennial. The seasonal variation of upwelling in the equatorial lower stratosphere shows a maximum during the northern fall-winter season, which is explained by a superposition of upward wave momentum

0148-0227/03/2003JD003871$09.00

flux in both hemispheres. The maximum momentum flux in the Northern Hemisphere is observed during November–March and in the Southern Hemisphere during September–November, so the total momentum flux of both hemispheres shows continuous large values from September to March [e.g., *Randel et al.*, 2002, hereinafter referred to as R02]. This wave drag variation produces the corresponding seasonal variation of temperature in the lower stratosphere [*Reed and Vlcek*, 1969; *Yulaeva et al.*, 1994]. The quasi-biennial oscillation (QBO) in the meridional circulation shows a well-defined two-cell structure symmetric with respect to the equator, related to the zonal wind direction and temperature [*Plumb and Bell*, 1982; *Dunkerton*, 1985]. However, an asymmetric structure is pronounced during the solstitial seasons, such that the winter cell extends to higher latitudes while the summer one almost disappears. The asymmetry can be explained by meridional transport of the QBO anomalies of angular momentum due to the meridional wind from the summer to the winter hemisphere [e.g., *Baldwin et al.*, 2001].

[4] These kinds of variations in tropical upwelling are indirectly estimated from the examination of radiative heating rates or wave forcing for seasonal cycle [e.g., *Rosenlof and Holton*, 1993; *Rosenlof*, 1995; *Eluszkiewicz et al.*, 1996; R02] and for the QBO [*Randel et al.*, 1999]. However, both the calculations include large uncertainties in the equatorial lower stratosphere. The radiative heating rate is quite small because the equatorial lower stratosphere approaches the equilibrium temperature. So the temperature difference near the QBO shear region or the tropical tropopause region leads to larger percentage difference of heating rate and also the residual circulation in the lower stratosphere. There are other major uncertainties in aerosol heating effect and tropospheric cloudiness in the equatorial lower stratosphere [*Olaguer et al.*, 1992; *Eluszkiewicz et al.*, 1997]. With respect to the calculation of wave forcing, on the other hand, the absolute vorticity vanishes in the deep tropics, which makes it difficult to calculate the latitudinal distribution of the tropical upwelling.

[5] Stratospheric measurements of water vapor (H_2O) and methane (CH_4) by the Halogen Occultation Experiment (HALOE) on board the Upper Atmosphere Research Satellite (UARS) have revealed seasonal variation of total hydrogen $[H_2O] + 2[CH_4]$ ($\hat{H}$) since 1991 (Figure 1) and provide a valuable opportunity to estimate the dynamical properties, such as ascent rate, horizontal and vertical mixing, and empirical age spectrum [e.g., *Mote et al.*, 1996]. *Mote et al.* [1998] deduced a time mean vertical distribution of upwelling, vertical diffusion and horizontal attenuation simultaneously from $\hat{H}$ and methane data by applying a simple one-dimensional model, and showed vertical velocity in a good agreement with the results derived from the calculation of radiative heating. Some extensive studies succeeded in deriving seasonal cycle and the QBO component in the tropical upwelling using water vapor profiles of the HALOE and in situ measurements, respectively [*Mote et al.*, 1996; *Andrews et al.*, 1999; *Niwano and Shiotani*, 2001]. However, these studies did not make a full spectral analysis of ascent rate of $\hat{H}$ as a function of latitude and altitude.

[6] In this study, we infer ascent rate from the annually varying signature of $\hat{H}$ in the tropical lower stratosphere, and describe the variations in terms of latitude, altitude, and frequency. The analysis of the frequency is focused on seasonal and interannual variations using HALOE data. The tropical isolation from midlatitudes, reported by various studies [*Plumb*, 1996; *Andrews et al.*, 2001; *Haynes and Shuckburgh*, 2000], backs up our estimation of the ascent rate from $\hat{H}$ data in the tropical lower stratosphere within the subtropical barriers. First, the satellite, rawinsonde and reanalysis data used in this study and the method of estimating the ascent rate are described in section 2. In section 3 the derived ascent rate then is shown for both the seasonal and QBO components. The validity of estimating ascent rate, and the relationship between variations in ascent rate and temperature are discussed in section 4. Finally, a summary is given in section 5.

2. Data and Methods

2.1. HALOE Trace Gas Data

[7] In this study, we use the H_2O and CH_4 profiles by the HALOE version 19 data from November 1991 to December 1999. Long term observations from HALOE provide continuous and high quality data, as summarized by *Russell et al.* [1993]. The V19 data of H_2O and CH_4 have an accuracy of ±5–10% [*Dessler and Kim*, 1999], which is similar to that of the V17 data reported by *Harries et al.* [1996] and *Park et al.* [1996]. The previous H_2O retrieval method (V18) had large differences between sunrise and sunset observations, while the sunrise/sunset differences for the V19 H_2O data have been significantly reduced (E. E. Remsberg, personal communication, 2002). A further comparison of HALOE V19 H_2O with data from other satellite, balloonborne, and aircraft measurements, is included in the Stratospheric Processes and Their Role in Climate (SPARC) water vapor assessment report [*Kley et al.*, 2000].

[8] The HALOE water vapor data have a dry bias of 5–20% between 60 and 100 hPa compared with aircraft or balloon measurements [*Kley et al.*, 2000]. *Randel et al.* [2001] noted that this dry bias may be partly caused by errors in the temperature-dependent O_2 continuum absorption, which is used in the V19 HALOE retrieval. The V19 retrieval of HALOE data shows that $\hat{H}$ at lower latitudes decreases above 40 hPa in the stratosphere with height [*Kley et al.*, 2000], and correspondingly that the effective yield of H_2O from CH_4 destruction is less than 2 in the lower stratosphere [*Dessler and Kim*, 1999], as previously suggested [*Le Texier et al.*, 1988]. However, it should be emphasized that time mean $\hat{H}$ may be vertically constant throughout the stratosphere within the accuracy of HALOE data.

[9] The HALOE data (level 2) are available on pressure levels of $1000 \times 10^{-(i/30)}$ hPa ($i = 0, 1, \ldots$), corresponding to a vertical spacing of about 0.5 km. HALOE instrument retrieves data in the tropics approximately 10 times per a year at sunrise and sunset events separately. For details of constructing zonal mean values with a latitudinal grid interval of 2.5 degrees, refer to *Niwano and Shiotani* [2001]. The mean seasonal cycle is calculated by sampling raw data on each calendar month, based on the data only spanning January 1993 and December 1999, because data are sparse under a condition of enhanced Pinatubo aerosol concentration in the lower stratosphere. If there are fewer

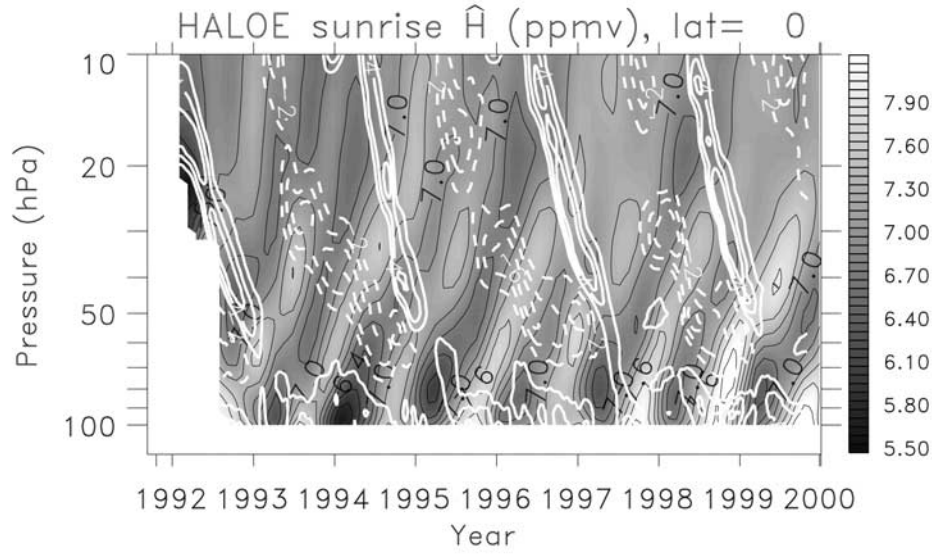

Figure 1. Pressure-time sections of HALOE $\hat{H}$ at the equator (colors and black contours). Vertical shear of zonal wind in Singapore is also plotted (white contours). Contour intervals are 0.3 ppmv for $\hat{H}$, and 2.0 m s^{-1} km^{-1} for vertical shear of zonal wind, with zero contours omitted. Negative values are denoted by dashed contours. See color version of this figure at back of this issue.

than two HALOE soundings in a particular month, the values for that month are found by linearly interpolating with respect to month. After then, we smooth the data with respect to time, by applying a 1-2-1 filter. Finally, the monthly data for both sunrise and sunset measurements are combined. One reason why both data are combined at the last step is a systematic difference between sunrise and sunset measurements for $\hat{H}$ data, while the ascent rate shows only a random difference. Another is that the ascent rate calculation using $\hat{H}$ in sunrise and sunset data separately raises significance of the ascent rate data.

[10] The mean seasonal cycle is subtracted from the original data to provide the interannual variation data. The interannual anomalies from the climatological annual cycle are regarded as the QBO variations in this study, because the variation is consistent with the QBO in the zonal wind and temperature fields. The QBO component in the ascent rate is discussed in the zonal mean field, because the QBO variation generally shows zonally uniform phase change in the tropical lower stratosphere [*Shiotani*, 1992; *Shiotani and Hasebe*, 1994].

2.2. Singapore Rawinsonde Data and UK Met Office Data

[11] In addition to HALOE trace gas data, temperature and zonal wind from Singapore rawinsonde data and the UK Met Office (UKMO) stratosphere-troposphere assimilation [*Swinbank and O'Neil*, 1994] spanning November 1991 and December 1999 are used in this study. Singapore data used here consist of data at the standard and significant levels, and are interpolated to the same pressure levels as for the HALOE data. In this study daily data are formed from original twice daily data and then smoothed with a low-pass filter designed to exclude periods less than 90 days. After the seasonal cycle is calculated at daily resolution from the smoothed data, deviations from the seasonal cycle (hereafter denoted as the QBO component) are obtained by subtracting seasonal cycle data from the smoothed daily data.

[12] The UKMO data are provided with a grid interval of 3.75° × 2.5° longitude-latitude and ~2.5 km log-pressure level. Zonal mean zonal wind and temperature are calculated on each day, and then seasonal cycle and deviations from it are derived in the same way as Singapore data. The original and anomaly data at daily resolution are smoothed by the 31-day running mean to cut off variations with higher frequency. For consistency, the data are selected only on days when the HALOE instrument retrieves data, and smoothed with a 1-2-1 filter, such that low-frequency variations close to Singapore data are provided.

[13] In the present study, Singapore data are used to compare with the ascent rate over the equator, while UKMO data are shown to examine the latitude distribution of the ascent rate. We should take it into account for a quantitative discussion that UKMO temperature data underestimate the amplitude of the QBO component compared to Singapore temperature data [*Randel et al.*, 1999].

2.3. Ascent Rate of $\hat{H}$ Anomalies

[14] The $\hat{H}$ anomalies are considered to be generated around the tropical tropopause region through the dehydration process, and afterward transported vertically by the upward branch of the Brewer-Dobson circulation, as seen in Figure 1. The tropical $\hat{H}$ anomalies ascend with time at a mean ascent rate of 0.2–0.3 mm s^{-1} (~10 km per year) within the subtropical barriers [*Mote et al.*, 1996; *Randel et al.*, 2001]. However, the ascending speed of the $\hat{H}$ anomalies can be modulated by the QBO and by seasonal variations. In Figure 1 it is clear that the passage of the QBO westerly shear zone (which corresponds to descent anomalies) prevents $\hat{H}$ anomalies from ascending around the 25 hPa level in the latter half of 1994 and 1996. The

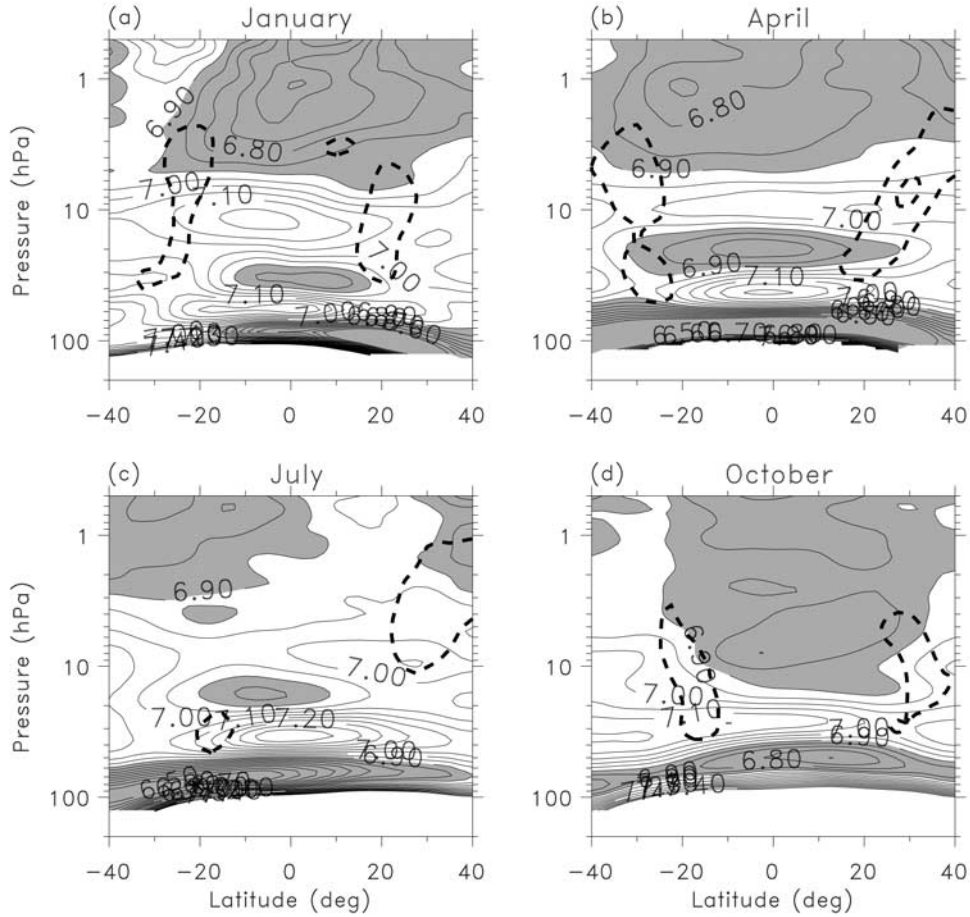

Figure 2. Cross sections of the climatological monthly mean $\hat{H}$ in (a) January, (b) April, (c) July, and (d) October, calculated from the HALOE measurements between 1993 and 1999. Contour interval is 0.05 ppmv, and values less than 6.9 ppmv are stippled. Dashed lines denote the 0.08 and 0.12 ppmv/5° contours of the CH_4 meridional gradient. Contours denoting values of <6.5 ppmv and >7.5 ppmv are omitted.

mean distribution of $\hat{H}$ (Figure 2) exhibits seasonal variation in the ascent rate of $\hat{H}$ anomalies, such that the positive anomaly reaches the 10-hPa level in January, higher than the level where the negative anomaly approaches in July (~20 hPa). Furthermore, an intriguing point is a meridional variation of the ascent rate of $\hat{H}$ confined to the equatorial latitudes within two regions of large meridional gradient of CH_4 in the subtropics, which means the position of the subtropical barriers. The isolation from midlatitudes means that the QBO and seasonal modulation in the ascent rate of $\hat{H}$ anomaly is mainly caused by vertical velocity variations.

[15] The ascent rate of $\hat{H}$ anomalies is estimated for every latitude, altitude and month by calculating a vertical lag-correlation between two vertical profiles of $\hat{H}$ at a certain time step (t_i) and the next time step (t_{i+1}). The calculation is based on the $\hat{H}$ data interpolated to a vertical grid interval of ~250 m. This vertical lag-correlation is calculated using vertical profiles with a vertical length of ~4 km below 30 hPa and ~6 km above 30 hPa. (The reason why $\hat{H}$ profile with a vertical length of 4 and 6 km is used is the balance of the gain and loss of the amount and quality of w_{tr} data. Actually, the 4- and 6-km vertical length of an $\hat{H}$ profile corresponds to about a half of vertical wavelength of tape recorder signal in $\hat{H}$ below and above 30 hPa, respectively.) The profile of $\hat{H}$ is considered to reach the height level at the next time step ($Z(p_{i+1}, t_{i+1})$) where the correlation coefficient becomes a maximum. So, the ascent rate is defined as the differential of the arrival altitude ($Z(p_{i+1}, t_{i+1}) - Z(p_i, t_i)$) with respect to time ($t_{i+1}$ and t_i).

[16] For the calculation of ascent rate, the $\hat{H}$ values are modified in the tropical lower stratosphere, so that the small bias (5–20%) of water vapor around 60–100 hPa [*Kley et al.*, 2000] is removed. The modified time mean value of $\hat{H}$ is defined in this study as below:

$$\tilde{\chi}(y,z,t) = \chi(y,z,t) - [\chi(y,z)] + [\chi_{\mathrm{MOD}}(y,z)], \qquad (1)$$

where

$$[\chi_{\mathrm{MOD}}(y,z)] = (1-a)[\chi(y,z)] + a[\chi(y)]_{z30-50}. \qquad (2)$$

Here χ is the mixing ratio of $\hat{H}$, $[\cdot]$ means time mean, $[\chi(y)]_{z30-50}$ is the time mean value of χ averaged in the range of 30–50 hPa, and the modified factor $a = 0.8$, so that $[\chi_{\mathrm{MOD}}]$ becomes 0.3–0.4 ppmv larger than the HALOE time mean $[\chi]$ in the lower stratosphere (~10% larger for H_2O). The change of the time mean value has a small effect

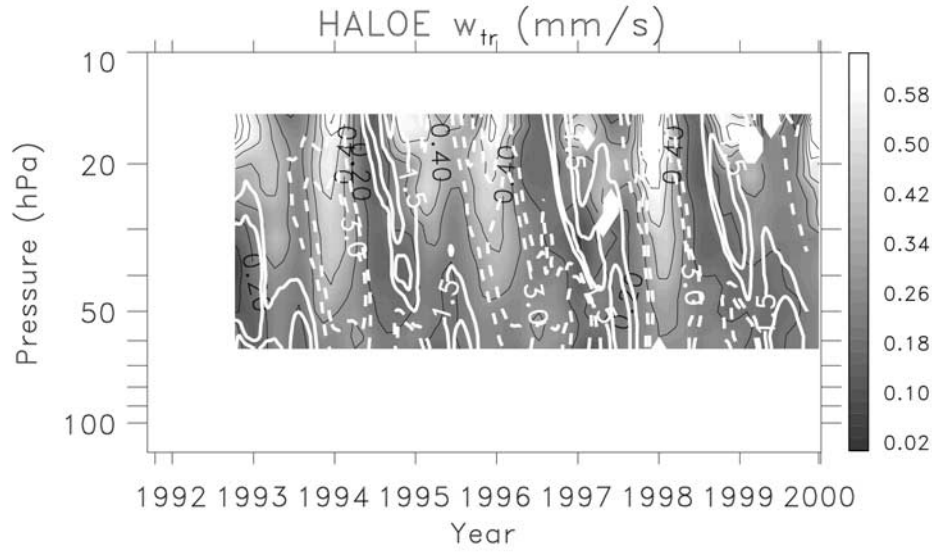

Figure 3. Pressure-time sections of w_{tr} at the equator (colors and black contours). Temperature in Singapore is also plotted at the equator (white contours). Here time mean values of temperature are subtracted from raw values. Contour intervals are 0.1 mm s^{-1} (black) and 1.5 K (white), with zero contours omitted. See color version of this figure at back of this issue.

on the phase of variations, such that the phase is pushed ahead by up to 2 months when changing a from 0 to 1. The ascent rate of the $\hat{H}$ anomaly is calculated from both sunrise and sunset data separately, and then both data are combined with each other. So the time mean value should be accurate in order to derive the ascent rate of $\hat{H}$.

[17] In this study the obtained results are shown in the region only above the ~60 Pa level, because $\hat{H}$ cannot be completely preserved due to the occurrence of dehydration up to the level of 80 hPa (the level of 60 hPa is 2 km above the 80 hPa level). This cirrus occurrence can be seen in aerosol extinction of Stratospheric Aerosol and Gas Experiment (SAGE) II and HALOE measurements [e.g., *Wang et al.*, 1996; *Massie et al.*, 2002].

[18] Several recent studies of tracer fields have shown that the tropical lower stratosphere around 20–60 hPa is a very quiet world isolated from the extratropics with subtropical barriers [*Andrews et al.*, 2001; *Haynes and Shuckburgh*, 2000], and is dominated by upward advection in a good approximation [*Plumb*, 1996; *Mote et al.*, 1998]. The subtropical barrier in the summer hemisphere is not merely a remnant of the winter strong barrier, but also is maintained by upwelling in the summer low latitude [*Neu et al.*, 2003]. However, the winter subtropical barrier is produced both by isentropic mixing and upward advection. Its position does not correspond to the maximum meridional gradient of vertical velocity [*Plumb*, 2002], but to the zero line of zonal mean wind much better [*Haynes and Shuckburgh*, 2000]. These studies support the notion that the ascent rate obtained from $\hat{H}$ seasonal cycle is a good indicator of the Lagrangian vertical velocity in the region bounded by the subtropical barriers.

3. Variability of Ascent Rates

3.1. Total Variability

[19] It is clear that the equatorial ascent rate of $\hat{H}$ (Figure 3) exhibits mainly two kinds of variations. One is the seasonal cycle with a maximum of 0.2–0.4 mm s^{-1} during December–January and a minimum of ~0.2 mm s^{-1} for June–July, and its amplitude is increasing with height. The other is a variation with a period of about two years, which is closely connected with the quasi-biennial oscillation (QBO). The ascent rate variation is about out of phase with the temperature variation, but the descent anomalies appear to precede warm anomalies. The features for the time mean value, and amplitude and phase of QBO variations generally agrees with results by *Niwano and Shiotani* [2001]. However, seasonal variation is newly retrieved in this study because the calculation of w_{tr} is based on $\hat{H}$ data including time mean value, instead of excluding time mean value in *Niwano and Shiotani* [2001]. The detail of difference between results from the two studies will be discussed in section 4.

[20] The amplitudes of the seasonal and interseasonal components are compared with each other in Figure 4. Note that the interseasonal component is defined by deviations from the seasonal cycle, and is tightly connected with the QBO, as seen in Figure 3. The amplitude is regarded as the standard deviation of each component multiplied by a factor $\sqrt{2}$ in this paper, because one standard deviation of a sinusoidal wave is equal to $1/\sqrt{2}$ of the original amplitude [*Randel et al.*, 1999; *Niwano and Shiotani*, 2001].

[21] The total amplitude shows an increase with height regardless of latitude, ranging from 0.06 mm s^{-1} at 60 hPa to 0.2 mm s^{-1} at 20 hPa. The two components have a similar amplitude around 30–40 hPa. However, it is notable that the spatial pattern of the two components exhibits different features. One is a vertical difference, such that the seasonal component is dominant in the upper region but the interannual component is prevail in the lower region. The other is a latitudinal difference. The interannual component is well confined to the tropics and ~0.4 mm s^{-1} (~40%) larger in tropics than in the southern subtropics in the region of 20–30 hPa. On the other hand, the seasonal component

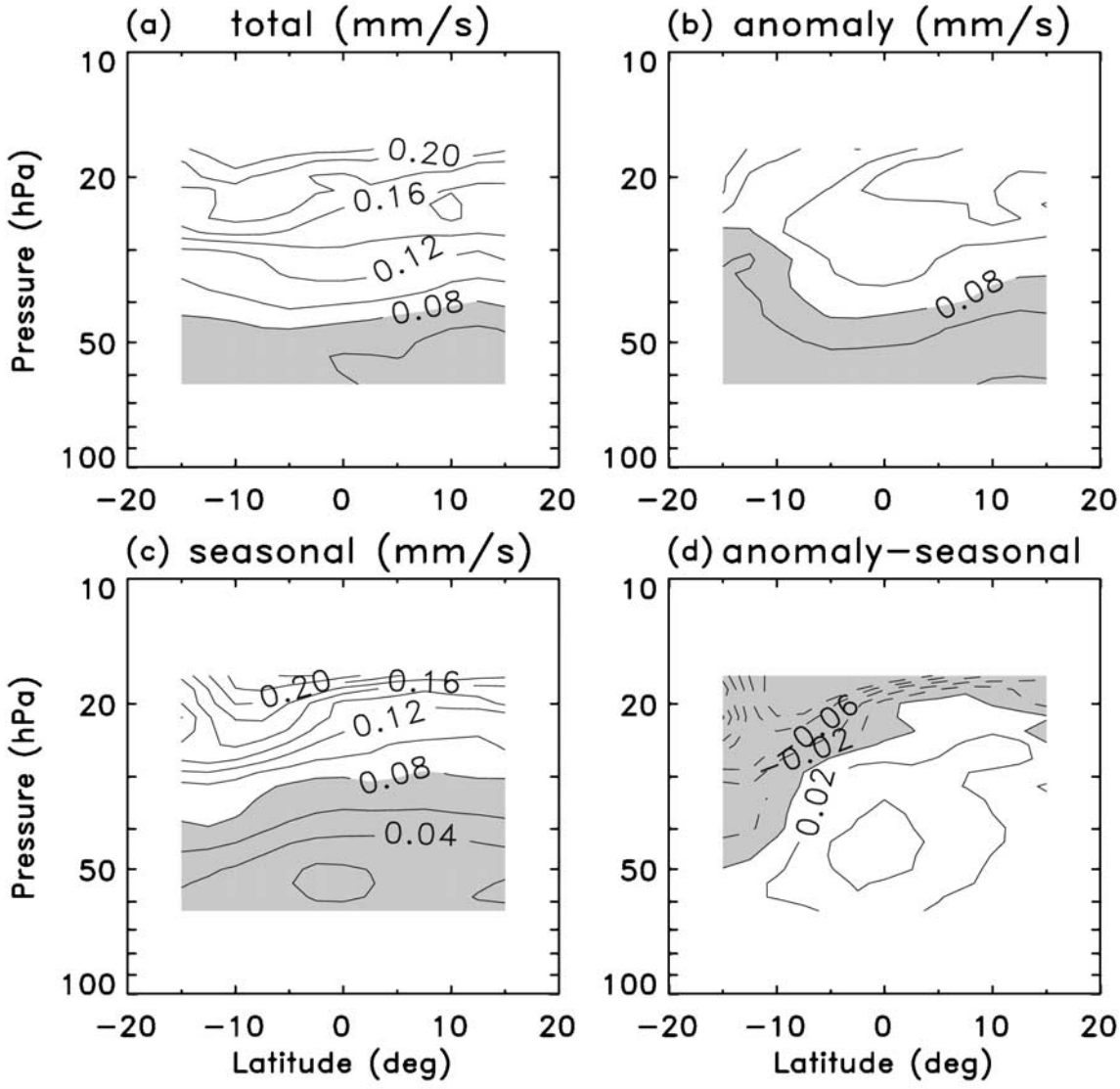

Figure 4. Amplitude of ascent rate w_{tr} with respect to (a) total, (b) interannual, and (c) seasonal components. Values less than 0.08 mm s^{-1} are stippled in Figures 4a–4c. The difference between seasonal and interannual components (Figure 4b minus Figure 4c) is also shown in Figure 4d. Negative values are stippled in Figure 4d. Contour intervals are 0.02 mm s^{-1}.

shows a uniform amplitude in the lower latitudes, but a variation ~0.6 mm s^{-1} (~50%) larger in the southern subtropics than other latitudes at the level of 20–30 hPa. The spatial difference between the amplitudes of the seasonal and interannual components can be confirmed in Figure 4d. The other important feature is a latitudinal tilt of anomalies; both amplitudes of the annual and interannual variation are tilting northward with height, as revealed in Figure 4d. The tilting feature of amplitude may be connected with the seasonal synchronization of the QBO [e.g., *Randel and Wu*, 1996].

3.2. Seasonal Cycle

[22] Hereafter, the seasonal and interannual components in the ascent rate of $\hat{H}$ are examined in order. First, the climatology of the ascent rate averaged within ±12.5° in January and July is shown in Figure 5. Note that maximum and minimum values of the seasonal cycle are observed around January and July. The ascent rate of $\hat{H}$ becomes 0.25–0.5 mm s^{-1} in January, and ~0.2 mm s^{-1} in July, so the ratio of the seasonal maximum to the minimum approaches ~2 above 35 hPa. An intriguing point is that w_{tr} is roughly constant in July. The values are in accordance with other results [*Eluszkiewicz et al.*, 1996; *Seol and Yamazaki*, 1999; *Randel and Newman*, 1999] (Table 1). A tendency to underestimate the seasonal amplitude is observed below 45 hPa in our results.

[23] In Figure 5, for a comparison of time mean values, the result obtained by *Mote et al.* [1998] is also plotted, which are derived from HALOE $\hat{H}$ data decomposed with the extended EOF. Their values generally agree with our results within the seasonal variations in our derived ascent rate, although showing some differences of ~0.05 mm s^{-1} below 46 hPa and above 25 hPa (which are discussed in

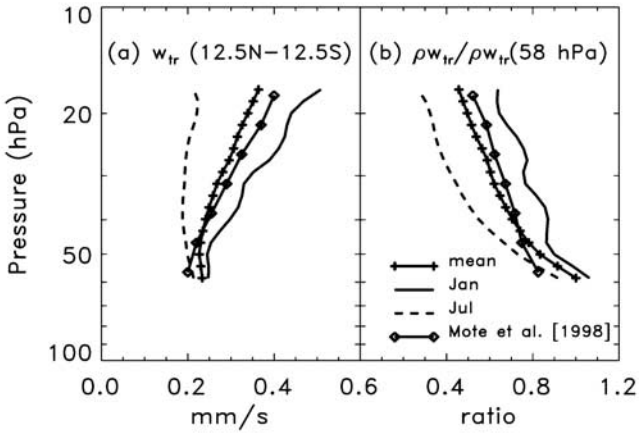

Figure 5. (a) Vertical profile of w_{tr} and (b) ratio of vertical mass flux to the time mean value at 58 hPa, which are averaged within ±12.5°. Solid lines with plus marks indicate time mean value. Solid and dashed lines denote the values in January and July, respectively. The result from *Mote et al.* [1996], which are averaged within ±12.0°, is denoted by solid line with diamonds for a comparison.

section 4). This good agreement encourages us to discuss observed seasonal and interannual variations as well as the time mean value.

[24] The corresponding vertical mass flux is calculated from the obtained ascent rate, to investigate how much mass flux is conserved at each level (Figure 5b). The vertical mass flux relative to the time mean value of $\rho_0 w_{tr}$ at 58 hPa shows a decrease with height because of the density factor. An intriguing point is the similarity in the decreasing mass flux above 40 hPa for January and July as well as for the time mean, although there is a large difference in a vertical increase of w_{tr} in January and July (Figure 5b). Considering the zonal momentum balance, horizontal attenuation of vertical mass flux can be driven by wave forcing plus zonal wind tendency [R02]. The observed values of mass attenuation rate in the range of 20–40 hPa suggest that the intrusion of the planetary waves into low latitudes (12.5°N and S) makes a relatively small difference between the values in January and July in this layer.

[25] Focusing on only the seasonal component, the vertical structure of the ascent rate and the temperature from Singapore are shown over the equator in Figure 6. The overall structure is that ascent anomalies are observed in the Northern Hemisphere winter, and descent anomalies in summer. The ascent rate variation is nearly anticorrelated with temperature variation at the first glance (Figure 6b). It however is noteworthy that the phase of the ascent rate is nearly constant, while the temperature phase delays as the height decreases. In the 40–60 hPa altitude range positive anomalies of the ascent rate appear during September–April, but precede the negative anomalies of temperature variations by 1–2 months.

[26] This phase relationship suggests that the radiative timescale becomes larger in the lower level. Considering the thermodynamic equation balance, this relationship can be accounted for by lifting the stratified isentropic surfaces by the ascent anomalies in a condition of radiative damping with a timescale shorter than the seasonal timescale. An additional comparison between temperature fields from Singapore rawinsonde data, the National Centers for Environmental Prediction (NCEP) reanalysis data, and the UK Met Office (UKMO) assimilation data, confirms that the phase for Singapore data is almost the same as the other two, although UKMO and NCEP temperature show seasonal amplitude ~30% smaller than that of Singapore temperature fields in the range of 20–60 hPa.

[27] Figure 7 presents the time-latitude section of seasonal variation including the time mean values at 31.6 hPa, where the seasonal cycle shows a well-established variation. At this level the ascent rate shows seasonal variation over the whole tropics with a maximum of ~0.35 mm s^{-1} in the northern winter and a minimum of ~0.20 mm s^{-1} in the northern summer. There is a latitudinal shift of the maximum upwelling region to low latitudes of the summer hemisphere as denoted by bullet symbols. The main point is the timing of the latitudinal shift. The shift is observed in equinoctal-solstitial season (March–June and July–August), which is earlier than the results from the calculation of radiative heating rates [e.g., *Randel and Newman*, 1999]. The other feature is a double-peak structure between 20 and 40 hPa only during November–February in Figure 7, which is also related to a quick and early latitudinal shift of maximum ascent rate. A similarity of this feature to the result from *Norton* [2001], who calculated ECMWF heating rates as a residual term, could suggest the connection between the double peak structure of residual vertical velocity and the tropospheric outgoing longwave radiation (OLR). Another possible explanation for the double peak structure is the planetary wave driving in the winter Northern Hemisphere. [*Plumb and Eluszkiewicz*, 1999; T. Iwasaki, personal communication, 2002]. The ascent rate anomalies driven by wave forcing in the winter-spring hemisphere can apparently produce the earlier latitudinal shift of the region with a maximum ascent rate. Other possibility is the fact that the QBO component in the ascent rates shows phase dependency of latitudinal scale [e.g., *Dunkerton and Delisi*, 1985]. Actually, the phase dependency of ascent rate is closely connected with the difference of vertical shear and acceleration of zonal wind between the QBO phases (cf. section 4.3). It however is kept in mind that the feature of the ascent rate w_{tr} may be only a remnant of the QBO.

Table 1. Vertical Velocity (mm s^{-1}) and the Ratio of the Minimum to Maximum

	This Study		RN99[a]	SY99[b]	
	31 hPa	46 hPa	50 hPa	30 hPa	50 hPa
DJF	0.36	0.26	0.3	0.37	0.27
MAM	0.30	0.23	0.25	0.26	0.18
JJA	0.21	0.20	0.2	0.26	0.20
SON	0.28	0.24	0.3	0.35	0.28
Mean	0.26	0.23	0.25	0.31	0.23
Ratio	1.7	1.3	1.5	1.4	1.6

[a]From *Randel and Newman* [1999], whose vertical velocity is derived from the calculation of radiation using the radiation code. The results are averaged within ±10°.

[b]From *Seol and Yamazaki* [1999], who examined mass flux of global upwelling from wave forcing at each altitude. Mass flux is transformed into velocity, supposed that mass flux is homogeneously distributed between 30°S and N.

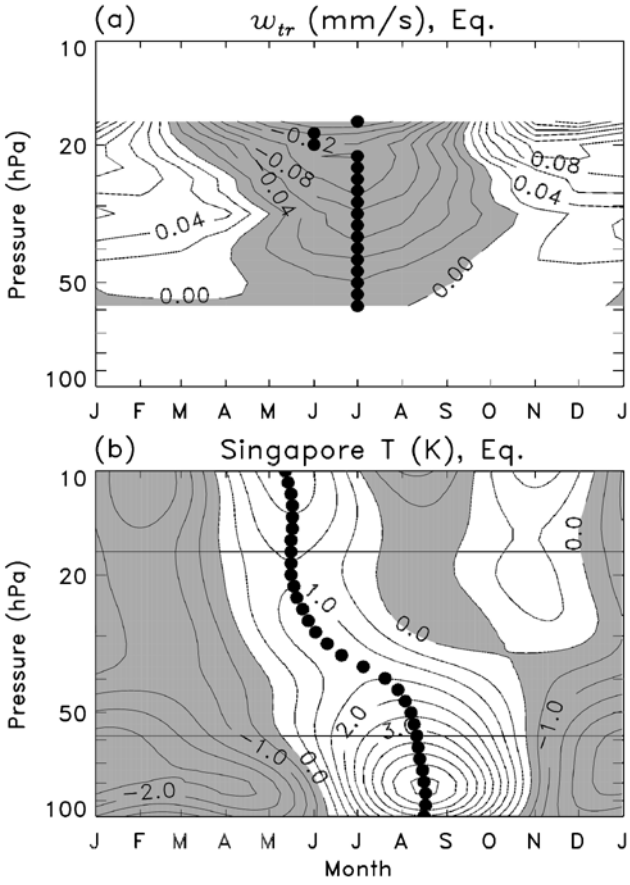

Figure 6. Climatological seasonal cycle of w_{tr} (mm s^{-1}) over (a) the equator and (b) temperature field (K) from Singapore rawinsonde data. Time mean value at each altitude is subtracted from the data. Contour intervals are 0.02 mm s^{-1} (Figure 6a) and 0.5 K (Figure 6b), respectively. Negative values are shaded, and bullets denote minimum ascent rate and maximum temperature at each level.

[28] The dominance of the annual amplitude in the Southern Hemisphere seen in Figure 4c is confirmed in Figure 7. The cause of the hemispheric difference in the seasonal amplitude can be examined by dividing the mean seasonal cycle into two components (Figure 8): the one is the symmetric component about the equator (the whole tropical annual cycle) and the other is the asymmetric component (latitudinal shift of large upwelling region). Both of the symmetric and asymmetric components show a peak in the Southern Hemisphere subtropics during the period of November–February. This phase overlap amplifies the seasonal cycle in the Southern Hemisphere, while weakening that in the Northern Hemisphere.

[29] The symmetric component of the seasonal cycle can be produced not by variations of ozone heating, but mainly by variation in the summation of wave damping in both hemispheres. On the other hand, the asymmetric component of ascent rate is involved with variations of the wave damping or the radiative forcing with a spring-summer maximum in one hemisphere. The dominance of the symmetric component in the seasonal cycle suggests that the wave damping possibly plays an important role in determining the vertical velocity in 20–60 hPa.

3.3. Interannual Variation

[30] Next, the interannual variation is examined to confirm how it is connected with the observed QBO component in the dynamical field. Figure 9 shows the time-altitude section of deviations from the climatological seasonal cycle (Figure 6). The variation exhibits a periodicity of two years in the whole altitude range, and a gradual downward propagation with time. The interannual variation increases with height and shows an amplitude exceeding 0.1 mm s^{-1} above 30 hPa (Figure 4). These values are generally consistent with the previous works by *Hasebe* [1994], *Randel et al.* [1999] and *Niwano and Shiotani* [2001]. However, the actual ascent rate could show a larger variation, because our estimate tends to underestimate a shallow structure of the ascent rate variation.

[31] The overall agreement between the variations of the ascent rate and temperature is observed, so that the ascent anomalies occur during the cold and easterly shear phase, and vice versa (Figure 1). However, there is a phase lag of 1–2 months between the descent anomalies and warm anomalies below 35 hPa. As well as the seasonal cycle, the transition from the out-of-phase to the quadrature relationship with the altitude decreasing implies that the radiative timescale becomes longer and closer to the timescale of seasonal variation ($360/2\pi \sim 60$ days) at lower altitudes. The detailed discussion about the radiative timescale is given in section 4.

[32] Figure 10 shows the time-latitude distribution of interannual variation of the ascent rate at 31.6 hPa, around which the amplitude has a maximum (Figure 4). The dominant variations with a periodicity of two years are observed in the equatorial region, and confined well to the equatorial latitudes. The interannual component roughly symmetric about the equator shows an amplitude with up to 0.1 mm s^{-1} at 31.6 hPa, which is larger than that for the symmetric component of seasonal cycle in Figure 8a ($\sim$0.06 mm s^{-1}). On the other hand, the tropical confinement of variations is observed only in the interannual components. The overall features agree with results derived from the radiative heating calculation [*Randel et al.*, 1999].

[33] A notable feature is the difference in the equatorial confinement of the descent and ascent anomalies. The descent anomalies exhibit a well-established variation which is symmetric about the equator, while the ascent anomalies present an equatorial asymmetric variation with a phase lag in latitude. This phase dependency of the ascent rate variation can be connected with the work of *Dunkerton and Delisi* [1985], which exhibited the phase dependency of the zonal wind acceleration, and a hemispheric asymmetry during the phase of the easterly acceleration (the easterly shear). In addition, several studies suggest that the meridional wind is important even over the equator in producing the secondary meridional circulation with a dominant cell in the winter hemisphere [*Randel et al.*, 1999; *Baldwin et al.*, 2001]. However, this phase dependency is different from temperature and ozone anomalies, which show symmetric variations [e.g., *Randel et al.*, 1999]. We should consider a balance among the momentum, thermodynamic and tracer continuity equations during the easterly acceleration phase.

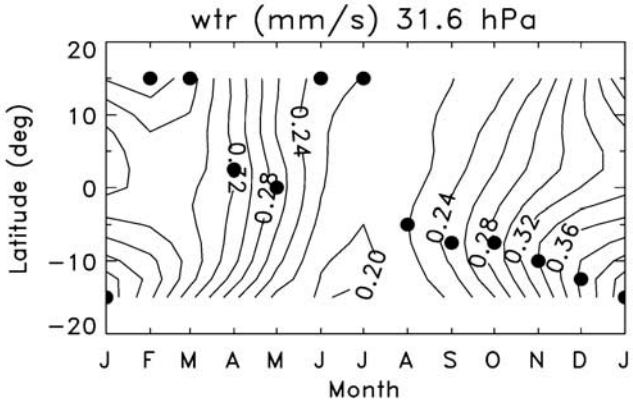

Figure 7. Climatological seasonal cycle of w_{tr} at 31.6 hPa (mm s^{-1}). Contour interval is 0.02 mm s^{-1}, and bullet symbols indicate the latitudes where ascent rate reaches a peak.

[34] In Figure 10, the ascent rate anomalies propagate downward more rapidly than temperature anomalies between 15 and 60 hPa. The rapid propagation raises a question how the vertical mass flux balances with the horizontal outflow. In order to examine the mass conservation for the interannual components, we compose the vertical mass flux with respect to the QBO phases. First we look for the times when ascent rate averaged between 10°S and 10°N reaches a local peak at 31.6 hPa between 1993 and 1999. Next we sum up three pairs of two year data with ascent rate maximum at 31.6 hPa in the middle.

[35] Figure 11 shows the vertical mass flux averaged within the range of 10°S–10°N. As seen in Figure 10, rapid downward propagation of ascent anomalies is observed between 20 and 50 hPa, but the amplitude maximum of $\rho_0 w_{tr}$ appears around 35–40 hPa (right panel) slightly lower than that in Figure 10. The meridional divergence is calculated from the mass weighted ascent rate at each altitude-time grid. The main point is a vertical phase propagation of horizontal mass flux, which is much slower than the propagation of vertical mass flux (bold contours). This is closely involved with that the maximum vertical mass flux is observed at the 35–40 hPa, and hence poleward flow is generated above maximum vertical mass flux while equatorward flow is below there. The resultant meridional attenuation of mass flux is large both above and below the amplitude maximum of vertical mass flux (right panel).

4. Discussion

4.1. An Estimate of Ascent Rate

[36] The obtained ascent rate w_{tr} of $\hat{H}$ anomalies is in general accordance with previous studies, but differences are observed in the time mean value, and latitudinal structure of seasonal and interannual components. Here the discrepancy is discussed in terms of seasonal and interannual variations.

4.2. Seasonal Cycle

[37] In section 3.2 the ascent rate shows some differences from other estimates; one is in the time mean value, and the other is in the timing of the latitudinal shift of maximum ascent rate. First, the time mean value was the same as the results by *Mote et al.* [1998] within an error bar, but these values are about 0.2 mm s^{-1} lower than the result derived from the calculation of radiative heating above 20 hPa [e.g., *Rosenlof*, 1995]. The region generally corresponds to where the vertical scale of vertical velocity becomes equivalent to the vertical scale of $\hat{H}$ seasonal anomalies. One is the upper region where the ascent rate rapidly increases with height, and the other is the region where a shallow structure of the ascent rate occurs in the shear region of the semi-annual oscillation and QBO. In the two regions, the ascent rate of time mean and seasonal cycle will be underestimated.

[38] Next, the latitudinal shift of large upwelling can be produced when Rossby waves and/or upward longwave flux from the troposphere affect the latitudinal distribution of $\hat{H}$. First, Rossby wave intrusion could produce the apparent ascent rate by homogenizing the tracer field and diminishing the latitudinal phase lag of $\hat{H}$ anomalies during the fall-spring season [*Ortland*, 1997; *Haynes and Shuckburgh*, 2000]. However, two issues should be additionally considered; the one is that Rossby wave breaking simultaneously drives the upward and downward mass flux equatorward and poleward of the breaking region respectively, the other is that our calculation is limited within the subtropical barriers, which corresponds to the equatorward boundary of the surf zone. Figure 2, actually, shows rapid uplift of

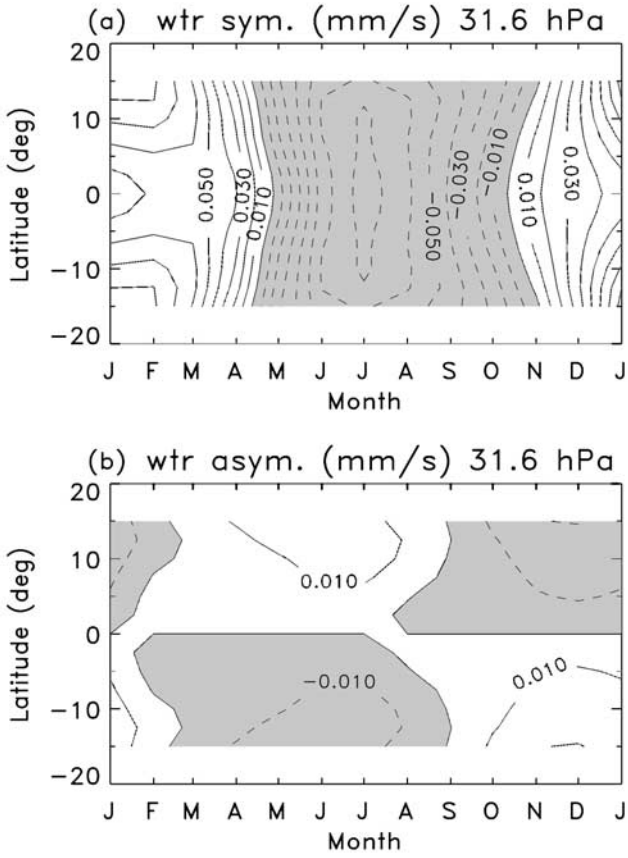

Figure 8. Same as Figure 7, but for (a) components symmetric and (b) asymmetric about the equator. Contour interval is 0.01 mm s^{-1}, with negative values are stippled.

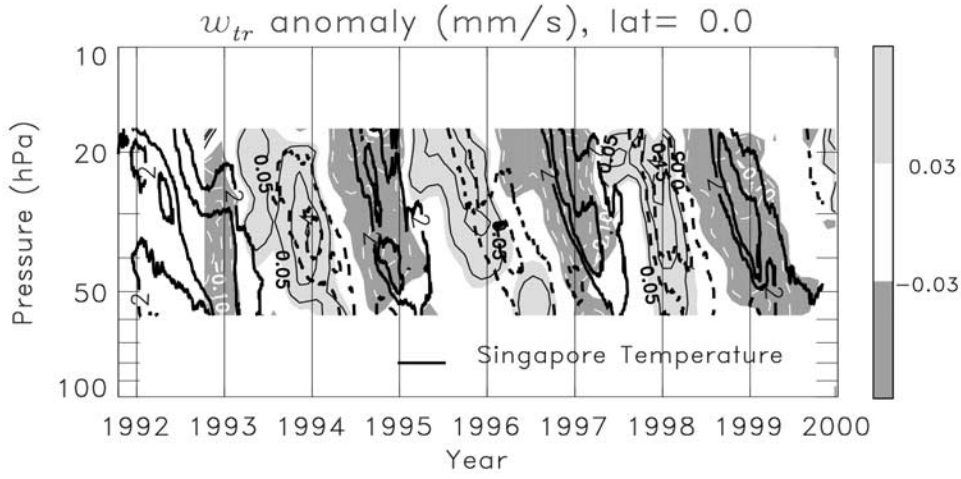

Figure 9. Interannual variation of ascent rates in mm s^{-1} (shaded, and thin contours) over the equatorial grid, defined by anomalies from climatological seasonal cycles in Figure 6. Contour interval is 0.05 mm s^{-1}, with the zero lines omitted. positive values (>0.03 mm s^{-1}) are lightly shaded, and negative values (<−0.03 mm s^{-1}) darkly shaded. Bold solid and dashed lines indicate the interannual variation of temperature field from Singapore rawinsonde data, and denote values of ±2 and ±4 K, respectively.

positive and negative anomalies of $\hat{H}$ at 0–15°N from January to April. The uplift of anomalies in the Northern Hemisphere is more rapid than that in the Southern Hemisphere, and is observed in the inside of the boundaries. These points support the spring latitudinal shift of maximum upwelling region.

[39] The second possibility of the spring latitudinal shift of large upwelling region is the latitudinal distribution of the upward radiative flux from the troposphere. Ozone absorbs the upward longwave flux from the troposphere at the 9.6 μm band. The absorption provides diabatic heating, and drives upwelling to be balanced with the heating. *Norton* [2001] reported a double peak structure of diabatic heating and vertical velocity in the northern winter using ECMWF reanalysis data. This result is closely connected with the upward radiative flux from the troposphere, such that in the lower stratosphere the equatorial air receives longwave radiation from high convective cloud top corresponding to low temperature, while the subtropical air absorbs longwave flux from Earth's surface corresponding to high temperature. However, *Olaguer et al.* [1992] did not report a double peak structure. One possibility of the discrepancy could be explained by uncertainties such as cloud properties, upper tropospheric water vapor. The way to parameterize the tropospheric cloud can affect the lower stratospheric adiabatic heating [*Norton*, 2001; K. H. Rosenlof, personal communication, 2003; T. Hirooka, personal communication, 2003].

4.3. Interannual Variation

[40] The interannual component in the present study shows a good agreement with the QBO amplitude in other studies [*Hasebe*, 1994; *Randel et al.*, 1999], but exhibits an amplitude ∼25% (corresponding to ∼0.075 mm s^{-1}) larger above 30 hPa than that estimated by *Niwano and Shiotani* [2001]. One reason for this discrepancy is related to the lag-correlation method, which uses vertical profiles of $\hat{H}$ within a certain range, and hence provides the ascent rate averaged in the range. If the vertical length of $\hat{H}$ is large enough to capture the vertical wavelength of $\hat{H}$ seasonal cycles, the

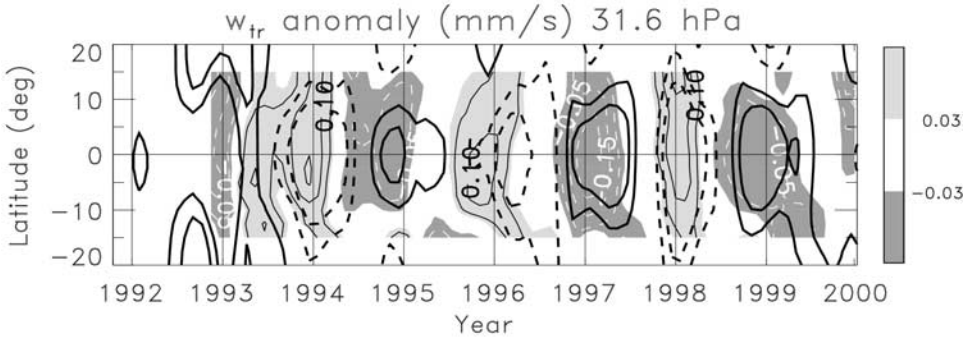

Figure 10. Latitude-time section of interannual variation of w_{tr} at 31.6 hPa (shaded, and thin lines). Counter interval is 0.05 mm s^{-1}, with the zero lines omitted. Negative values are indicated by thin dashed contours, and shaded. Bold solid and dashed lines denote interannual anomalies of temperature from UKMO data, and contours indicate ±2, ±4 K, respectively.

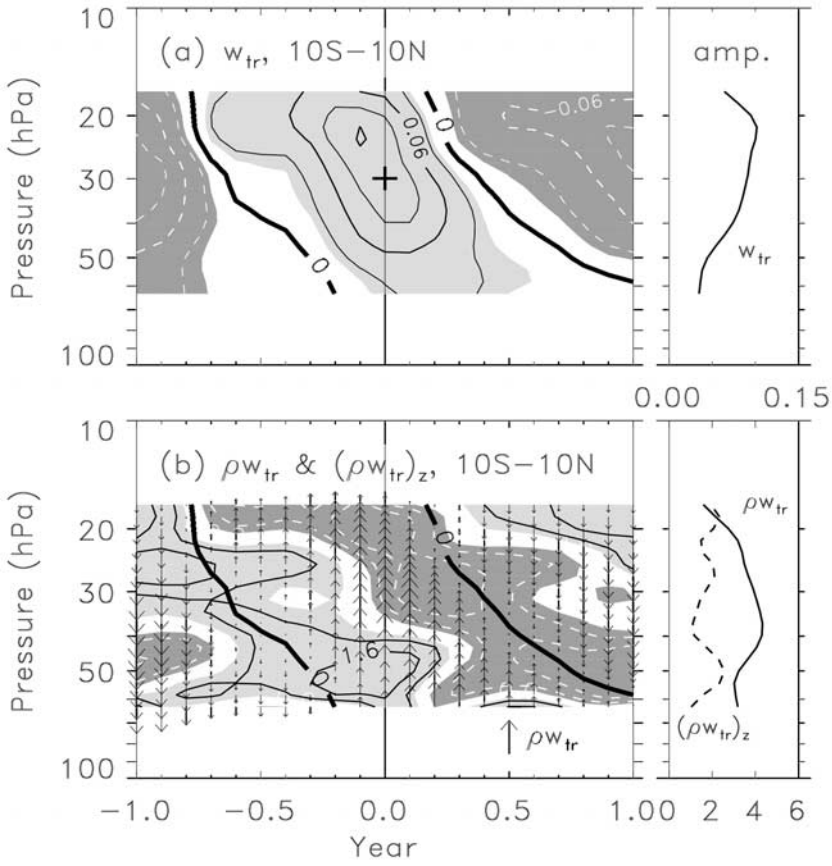

Figure 11. QBO composites which is constructed using the ascent rate at 31.6 hPa as a reference (plus symbol). (a) 10°S–10°N mean of the ascent rate w_{tr} (shaded, and thin contours) in the left panel, and its amplitude in unit of mm s^{-1} in the right panel. Contour interval is 0.03 mm s^{-1}. Negative values are dashed, with zero lines indicated by bold lines. Values less than -0.02 mm s^{-1} are darkly shaded, while more than 0.02 mm s^{-1} lightly shaded. (b) Same as Figure 11a, but for vertical mass flux $\rho_0 w_{tr}$ in unit of 10^{-6} kg m^{-2} s^{-1} (vectors) and its divergence $\partial(\rho_0 w_{tr})/\partial z$ in unit of 10^{-9} kg m^{-3} s^{-1} (thin contours, and shaded), in the left panel, and these amplitudes (denoted by solid and dashed lines, respectively) in the right panel. Contour intervals are 0.8×10^{-9} kg m^{-3} s^{-1}, with zero contours omitted. Vector length is presented by unit vector of 5.0×10^{-6} kg m^{-2} s^{-1}. Values less than -0.4×10^{-9} kg m^{-3} s^{-1} are darkly shaded, and larger than 0.4×10^{-9} kg m^{-3} s^{-1} lightly shaded. Thick solid lines are the same as in Figure 11a.

lag-correlation method is reliable even in the 20–30 hPa level, where the signal of $\hat{H}$ seasonal cycle becomes ambiguous. On the other hand, the method used by *Niwano and Shiotani* [2001] is effective in the altitude range where the seasonal component of $\hat{H}$ is well-structured so that the altitude where $\chi_z = 0$ and $\chi_{zt} = 0$ are uniquely determined. In the altitude range of 20–30 hPa, it would be ineffective and reduce the amplitude of variations more than that in this paper. Thus the lag-correlation method in the present study can capture the actual ascent rate variation in the upper region.

[41] The other effect is vertical and horizontal mixing, which can generate the apparent ascent rate of $\hat{H}$. The two types of mixing can appear in the wind shear region (for Rossby waves, see *Shuckburgh et al.* [2001]). If the horizontal mixing occurs over all the tropical latitudes, the QBO-related upward/downward displacement of $\hat{H}$ anomalies will be flattened in the meridional direction. The tropical mixing would result in underestimating the maximum and minimum ascent rate in the wind shear region over the equator. On the contrary, the vertical mixing contributes to an upward shift of $\hat{H}$ anomalies and hence false large ascent rate regardless of the wind direction of the zonal wind acceleration [*Mote et al.*, 1998]. As a result, it has little effect on the amplitude and phase of the QBO in the ascent rate.

4.4. A Relationship With Temperature Variation

[42] The derived information of the seasonal and QBO amplitudes of ascent rate is used to investigate the radiative timescale with a combination of temperature data on the basis of the thermodynamic equation. The thermodynamic equation is

$$\frac{\partial \bar{\theta}_\omega}{\partial t} + \overline{w}_\omega \bar{\theta}_{0z} = \overline{Q}. \tag{3}$$

The notation used here follows *Andrews et al.* [1987]. The variation of a quantity q is expressed by the summation of

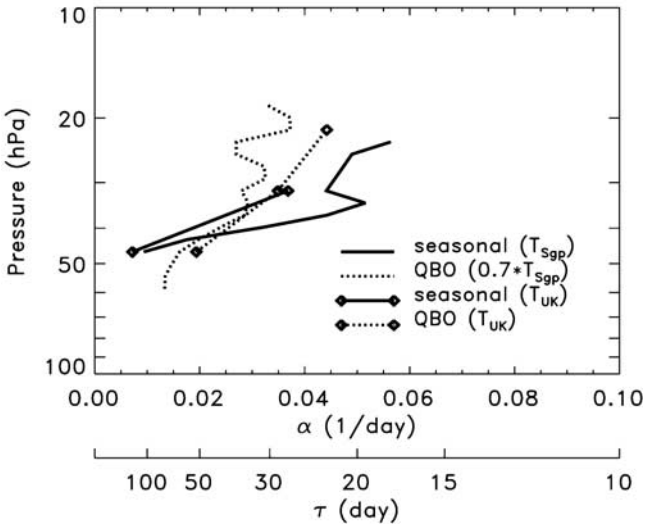

Figure 12. Regression coefficient α calculated from (3) over the equatorial latitude, using ascent rate and temperature both for the seasonal (solid lines) and QBO components (thick dotted lines). Temperature data are taken from Singapore rawinsonde data (lines without marks) and UKMO zonal mean data over the equator (lines with diamonds). The coefficient for the QBO in Singapore is calculated using temperature anomalies multiplied by 0.7, taking it into account that temperature variation over Singapore is probably larger the zonally averaged variation. If the correlation coefficient is less than 0.40 when α are calculated, α is not plotted.

the annual and QBO components as $q_\omega = q_A + q_B$. Here the horizontal advection has been neglected, and the diabatic heating term $Q = -\alpha(\overline{\theta}_\omega - \overline{\theta}_e)$ is expressed as a Newtonian cooling. The temporal variation of radiative equilibrium potential temperature $\overline{\theta}_e$ is approximated to be much smaller than that of $\overline{\theta}_\omega$ over the tropics.

[43] The radiative damping rate α can be then described in terms of each frequency ω, respectively:

$$\alpha(z) = -\frac{\overline{\theta}_{\omega t}(z,t) + \overline{w}_\omega(z,t)\overline{\theta}_{0z}(z)}{\overline{\theta}_\omega(z,t)}. \qquad (4)$$

[44] The radiative relaxation coefficient is obtained from a regression analysis between variations of the numerator and the denominator in the right hand side of equation (3). The vertical profile of the obtained coefficient is presented both in terms of the seasonal and QBO components, using Singapore and UKMO equatorial data (Figure 12). Here the QBO component in Singapore temperature data is multiplied by 0.7, taking into account the dominance of QBO component in Singapore rawinsonde data to UKMO zonal mean data [*Randel et al.*, 1999] and the underestimate of the QBO component of the ascent rate.

[45] Figure 12 shows the radiative damping coefficient α of 1/(20–30 day) in the 20–30 hPa layer and 1/(40–100 day) in the 40–60 hPa layer both in the cases of the seasonal and QBO components, and an increase of α with height. The general agreement of the radiative timescales estimated from the regression analysis and from the phase relationship (Figures 6 and 10) emphasizes that our estimate of the ascent rate is qualitatively and quantitatively reasonable with respect to temporal variations. This timescale observed in the layer of 40–60 hPa is close to the relaxation timescale of ~50–100 days obtained by *Mlynczak et al.* [1999] and R02 rather than that of ~30 days [*Newman and Rosenfield*, 1997], as summarized in Table 2.

[46] We emphasize that the observed downward propagation of temperature anomalies for the seasonal cycle in the lower stratosphere (Figure 6b) can be generated only by the vertical difference of radiative timescale, but without the downward propagation of ascent rate anomalies. The vertical difference of radiative timescale reaches about 100 days (15 days at 20 hPa and more than 100 days at 50 hPa). This value (~100 days) is consistent with observed vertical phase lag of temperature anomalies precede at 20 hPa relative to 60 hPa by 3 months. Corresponding well to this estimate, observed seasonal variation of the ascent rate shows a rapid downward propagation of anomalies from 15 hPa to 60 hPa (Figure 6a).

[47] The other feature is the difference in the damping timescale of seasonal and QBO components, such that the QBO component shows damping timescale shorter than the timescale of the seasonal cycle below about 40 hPa. This difference may be explained by two effects. One is the damping timescale which can depend on the vertical scale of the considered variation [e.g., *Alimandi and Visconti*, 1983]. The other is the effect of upward radiative flux from the troposphere on heating in the lower stratosphere through absorption by ozone at the 9.6-μm band [*Norton*, 2001]. The seasonal cycle of tropospheric radiative flux adds to the temperature-dependent longwave radiation in the lower stratosphere, so it may result in lengthening radiative timescale expressed in the form (3). Correspondingly, the correlation between two terms in (3) deteriorates below 50 hPa. This deteriorating correlation also supports the

Table 2. Infrared Radiative Relaxation Timescale

	This Study	R02[a]	NR97[b]	M99[c]
Timescale α, Day				
20–30 hPa	20–30	15–20	10–15	35–170
50–70 hPa	40–100	30–100	~24	70–300
Method	a regression of variations in temperature and ascent rate of $\hat{H}$ anomalies	a regression of temperature and residual vertical velocity obtained from wave forcing	a regression of temperature and radiative heating rate from the radiative calculation	a calculation of thermal perturbation of infrared radiative heating from the radiation calculation

[a]From *Randel et al.* [2001], who derived a tropical mean value averaged within ±15°.
[b]From *Newman and Rosenfield* [1997], who exhibits a tropical value in January.
[c]From *Mlynczak et al.* [1999], showing global mean values.

hypothesis that longwave radiative cooling can be affected by upward radiative flux from the troposphere.

5. Summary

[48] Seasonal and interannual variations of ascent rates have been examined using HALOE water vapor (H_2O) and methane (CH_4) data with respect to latitude and height. The ascent rate estimate is based on calculating the vertical lag-correlation of rising signals of variations in the entry value of $\hat{H}$ ($\equiv [H_2O] + 2[CH_4]$) (Figures 1 and 2). The derived ascent rate exhibits two kinds of dominant variations in the range of ±15° of the equator. The one is the QBO-related variation which is confined to the tropical latitudes, and the other is the seasonal variation with large amplitude in the subtropical Southern Hemisphere (Figures 3 and 4). We emphasize that the radiative timescale of 40 $\sim$ 100 days below 50 hPa is quite long compared with the previous studies (Figure 12), and the long timescale is confirmed by the consistency in the amplitude and phase of the seasonal and QBO variations in ascent rate and temperature.

[49] The seasonal cycle shows the vertically in-phase ascent (descent) anomalies in the Northern winter (summer) in the range of 20–40 hPa, and the ratio of the minimum to the maximum value is 1.5–2 (Figures 5 and 6). Below 40 hPa the phase slightly precedes that above 40 hPa, which implies that the nature of wave forcing to drive upwelling is different below and above the 40 hPa level. The ascent rate variation is roughly out-of-phase with the temperature variation, but the phase lag increases as the altitude decreases (Figure 5), which is closely connected with the radiative timescale. The seasonal cycle shows an early appearance of the summer maximum in the subtropics, and a double peak structure during the northern winter season (Figure 7). These two structures imply the existence of strong wave forcing in the winter hemisphere and/or upward radiative forcing from the troposphere, as producing the fine structures of ascent rate. A majority of the seasonal amplitude in the southern subtropics can be interpreted by the phase overlap of the equatorial symmetric and asymmetric components, with a maximum in the summer Southern Hemisphere (Figure 8).

[50] The interannual component is characterized by variations with a periodicity of about two years confined to the tropical latitudes opposite to the seasonal component. The QBO variation shows the nearly out-of-phase relationship between the ascent rate and temperature with a phase lag of 1–2 months in the lower altitudes (Figure 10). At 31.6 hPa the QBO component is dominant (an amplitude of 0.10 mm s^{-1}), while seasonal cycle is secondary (an amplitude of 0.06 mm s^{-1}). The downward propagation of ascent anomalies is more rapid than that of temperature variation, but mass attenuation estimated from vertical mass flux presents much slower downward propagation, as balanced with vertical mass flux (Figure 11). Furthermore, the QBO anomalies of the ascent rate show the dependency on the QBO phase: descent anomalies have a well-established equatorial symmetric structure, while ascent anomalies are asymmetric about the equator and propagate latitudinally (Figure 10). This phase dependency of the ascent rate variation can be closely connected with the phase dependency of zonal wind acceleration.

[51] **Acknowledgments.** The authors specially appreciate Hitoshi Mukougawa for constructive review of the doctoral thesis of the first author, which is the base of the present paper. They also thank Sigeo Yoden, William J. Randel, Matthew H. Hitchman, Nozomi Kawamoto, Takafumi Sugita, Hideharu Akiyoshi, Makoto Koike, Toshiki Iwasaki, Ellis E. Remsberg, John C. Gille, and two anonymous reviewers for valuable comments. Thanks are given Hiroo Hayashi for archiving the UK Met Office data. The research is financially supported by research fellowships of the Japan Society for the Promotion of Science for Young Scientists.

References

Alimandi, G., and G. Visconti, Radiative damping and amplitude of long-wavelength modes in the stratosphere, *J. Atmos. Sci.*, *40*, 2243–2250, 1983.

Andrews, A. E., K. A. Boering, B. C. Daube, S. C. Wofsy, E. J. Hintsa, E. M. Weinstock, and T. P. Bui, Empirical age spectra for the lower tropical stratosphere from in situ observations of CO_2: Implications for stratospheric transport, *J. Geophys. Res.*, *104*, 26,581–26,595, 1999.

Andrews, A. E., K. A. Boering, S. C. Wofsy, B. C. Daube, D. B. Jones, S. Alex, M. Loewenstein, J. R. Podolske, and S. E. Strahan, Empirical age spectra for the midlatitude lower stratosphere from in situ observations of CO_2: Quantitative evidence for a subtropical "barrier" to horizontal transport, *J. Geophys. Res.*, *106*, 10,257–10,274, 2001.

Baldwin, M. P., et al., The quasi-biennial oscillation, *Rev. Geophys.*, *39*, 179–229, 2001.

Dessler, A. E., and H. Kim, Determination of the amount of water vapor entering the stratosphere based on Halogen Occultation Experiment (HALOE) data, *J. Geophys. Res.*, *104*, 30,605–30,607, 1999.

Dunkerton, T. J., On the mean meridional mass motions of the stratosphere and mesosphere, *J. Atmos. Sci.*, *35*, 2325–2333, 1978.

Dunkerton, T. J., A two-dimensional model of the quasi-biennial oscillation, *J. Atmos. Sci.*, *42*, 1151–1160, 1985.

Dunkerton, T. J., and D. P. Delisi, Climatology of the equatorial lower stratosphere, *J. Atmos. Sci.*, *42*, 376–396, 1985.

Eluszkiewicz, J., et al., Residual circulation in the stratosphere and lower mesosphere as diagnosed from Microwave Limb Sounder data, *J. Atmos. Sci.*, *53*, 217–240, 1996.

Eluszkiewicz, J., D. Crisp, R. G. Grainger, A. Lambert, A. E. Roche, J. B. Kumer, and J. L. Mergenthaler, Sensitivity of residual circulation diagnosed from the UARS data to the uncertainties in the input fields and to the inclusion of aerosols, *J. Atmos. Sci.*, *54*, 1739–1757, 1997.

Harries, J. E., J. M. Russell III, A. F. Tuck, L. L. Gordley, P. Purcell, K. Stone, R. M. Bevilacqua, M. Gunson, G. Nedoluha, and W. A. Traub, Validation of measurements of water vapor from the Halogen Occultation Experiment, *J. Geophys. Res.*, *101*, 10,205–10,216, 1996.

Hasebe, F., Quasi-biennial oscillation of ozone and diabatic circulation in the equatorial stratosphere, *J. Atmos. Sci.*, *51*, 1238–1242, 1994.

Haynes, P. H., and E. F. Shuckburgh, Effective diffusivity as a diagnostic of atmospheric transport: 1. Stratosphere, *J. Geophys. Res.*, *105*, 22,795–22,810, 2000.

Kley, D., J. M. Russell III, and C. Phillips, Stratospheric processes and their role in climate (SPARC) assessment of upper tropospheric and stratospheric water vapour, *SPARC Rep. 2, WCRP-113, WMO/TD-1043*, World Clim. Res. Prog., World Meteorol. Org., Geneva, 2000.

Le Texier, H., S. Solomon, and R. R. Garcia, The role of molecular hydrogen and methane oxidation in the water vapour budget of the stratosphere, *Q. J. R. Meteorol. Soc.*, *114*, 281–295, 1988.

Massie, S., A. Gettelman, W. Randel, and D. Baumgardner, Distribution of tropical cirrus in relation to convection, *J. Geophys. Res.*, *107*(D21), 4591, doi:10.1029/2001JD001293, 2002.

Mlynczak, M. G., C. J. Mertens, R. R. Garcia, and R. W. Portmann, A detailed evaluation of the stratospheric heating budget: 2. Global radiation balance and diabatic circulations, *J. Geophys. Res.*, *104*, 6039–6066, 1999.

Mote, P. W., K. H. Rosenlof, M. E. McIntyre, E. S. Carr, J. C. Gille, J. R. Holton, J. S. Kinnersley, H. C. Pumphrey, J. M. Russell III, and J. W. Waters, An atmospheric tape recorder: The imprint of tropical tropopause temperatures on stratospheric water vapor, *J. Geophys. Res.*, *101*, 3989–4006, 1996.

Mote, P. W., T. J. Dunkerton, M. E. McIntyre, E. A. Ray, and P. H. Haynes, Vertical velocity, vertical diffusion, and dilution by midlatitude air in the tropical lower stratosphere, *J. Geophys. Res.*, *103*, 8651–8666, 1998.

Neu, J. L., L. C. Sparling, and R. A. Plumb, Variability of the subtropical "edges" in the stratosphere, *J. Geophys. Res.*, *108*(D15), 4482, doi:10.1029/2002JD002706, 2003.

Newman, P. A., and J. E. Rosenfield, Stratospheric thermal damping times, *Geophys. Res. Lett.*, *24*, 433–436, 1997.

Niwano, M., and M. Shiotani, Quasi-biennial oscillation in vertical velocity inferred from trace gas data in the equatorial lower stratosphere, *J. Geophys. Res.*, *106*, 7281–7290, 2001.

Norton, W. A., Longwave heating of the tropical lower stratosphere, *Geophys. Res. Lett.*, *28*, 3653–3656, 2001.
Olaguer, E. P., H. Yang, and K. K. Tung, A re-examination of the radiative balance of the stratosphere, *J. Atmos. Sci.*, *49*, 1242–1263, 1992.
Ortland, A. D., Rossby wave propagation into the tropical stratosphere observed by the High Resolution Doppler Imager, *Geophys. Res. Lett.*, *24*, 1999–2002, 1997.
Park, J. H., et al., Validation of Halogen Occultation Experiment CH_4 measurements from the UARS, *J. Geophys. Res.*, *101*, 10,183–10,204, 1996.
Plumb, R. A., A "tropical pipe" model of stratospheric transport, *J. Geophys. Res.*, *101*, 3957–3972, 1996.
Plumb, R. A., Stratospheric transport, *J. Meteorol. Soc. Jpn.*, *80*, 793–809, 2002.
Plumb, R. A., and R. C. Bell, A model of the quasi-biennial oscillation on an equatorial beta-plane, *Q. J. R. Meteorol. Soc.*, *108*, 335–352, 1982.
Plumb, R. A., and J. Eluszkiewicz, The Brewer-Dobson circulation: Dynamics of the tropical upwelling, *J. Atmos. Sci.*, *56*, 868–890, 1999.
Randel, W. J., and P. A. Newman, The Stratosphere in the Southern Hemisphere, in *Meteorology of the Southern Hemisphere*, *AMS Monogr. Ser.*, vol. 27, chap. 6, pp. 243–282, Am. Meteorol. Soc., 1999.
Randel, W. J., and F. Wu, Isolation of the ozone QBO in SAGE II data by singular value decomposition, *J. Atmos. Sci.*, *53*, 2546–2559, 1996.
Randel, W. J., F. Wu, R. Swinbank, J. Nash, and A. O'Neil, Global QBO circulation derived from UKMO stratospheric analyses, *J. Atmos. Sci.*, *56*, 457–474, 1999.
Randel, W. J., F. Wu, A. Gettelman, J. M. Russell III, J. M. Zawodny, and S. J. Oltmans, Seasonal variation of water vapor in the lower stratosphere observed in Halogen Occultation Experiment data, *J. Geophys. Res.*, *106*, 14,313–14,325, 2001.
Randel, W. J., R. R. Garcia, and F. Wu, Time-dependent upwelling in the tropical lower stratosphere estimated from the zonal-mean momentum budget, *J. Atmos. Sci.*, *59*, 2141–2152, 2002.
Reed, R. J., and C. L. Vlcek, The annual temperature variation in the lower tropical stratosphere, *J. Atmos. Sci.*, *26*, 163–167, 1969.
Rosenlof, K. H., Seasonal cycle of the residual mean circulation in the stratosphere, *J. Geophys. Res.*, *100*, 5173–5191, 1995.
Rosenlof, K. H., and J. R. Holton, Estimates of the stratospheric residual circulation using the downward control principle, *J. Geophys. Res.*, *98*, 10,465–10,479, 1993.
Russell, J. M., III, L. L. Gordley, J. H. Park, S. R. Drayson, W. D. Haskett, R. J. Cicerone, A. F. Tuck, J. E. Frederick, J. E. Harries, and P. J. Crutzen, The Halogen Occultation Experiment, *J. Geophys. Res.*, *98*, 10,777–10,797, 1993.
Semeniuk, K., and T. G. Shepherd, Mechanism for tropical upwelling in the stratosphere, *J. Atmos. Sci.*, *58*, 3097–3115, 2001.
Seol, D.-I., and K. Yamazaki, Residual mean meridional circulation in the stratosphere and upper troposphere: Climatological aspects, *J. Meteorol. Soc. Jpn.*, *77*, 985–996, 1999.
Shiotani, M., Annual, quasi-biennial, and El Niño-Southern Oscillation (ENSO) timescale variations in equatorial total ozone, *J. Geophys. Res.*, *97*, 7625–7633, 1992.
Shiotani, M., and F. Hasebe, Stratospheric ozone variations in the equatorial region as seen in SAGE data, *J. Geophys. Res.*, *99*, 14,575–14,584, 1994.
Shuckburgh, E. F., W. A. Norton, A. M. Iwi, and P. H. Haynes, The influence of the quasi-biennial oscillation on isentropic transport and mixing in the tropics and subtropics, *J. Geophys. Res.*, *106*, 14,327–15,337, 2001.
Swinbank, R., and A. O'Neil, A stratosphere-troposphere data assimilation system, *Mon. Weather Rev.*, *122*, 686–702, 1994.
Wang, P.-H., P. Minnis, M. P. McCormick, G. S. Kent, and K. M. Skeens, A 6-year climatology of cloud occurrence frequency from Stratospheric Aerosol and Gas Experiments (1985–1990), *J. Geophys. Res.*, *101*, 20,407–29,429, 1996.
Yulaeva, E., J. R. Holton, and J. M. Wallace, On the cause of the annual cycle in the tropical lower stratospheric temperature, *J. Atmos. Sci.*, *51*, 169–174, 1994.

M. Niwano, Department of Geophysics, Kyoto University, Kita-shirakawa-oiwake-cho, Kyoto 606-8502, Japan. (niwano@kugi.kyoto-u.ac.jp)
M. Shiotani, RASC, Kyoto University, Gogajo, Uji, Kyoto 611-0011, Japan. (shiotani@kurasc.kyoto-u.ac.jp)
K. Yamazaki, Graduate School of Environmental Earth Science, Hokkaido University, Kita 10 Nishi 5, Kita, Sapporo 060-0810, Japan. (yamazaki@ees.hokudai.ac.jp)

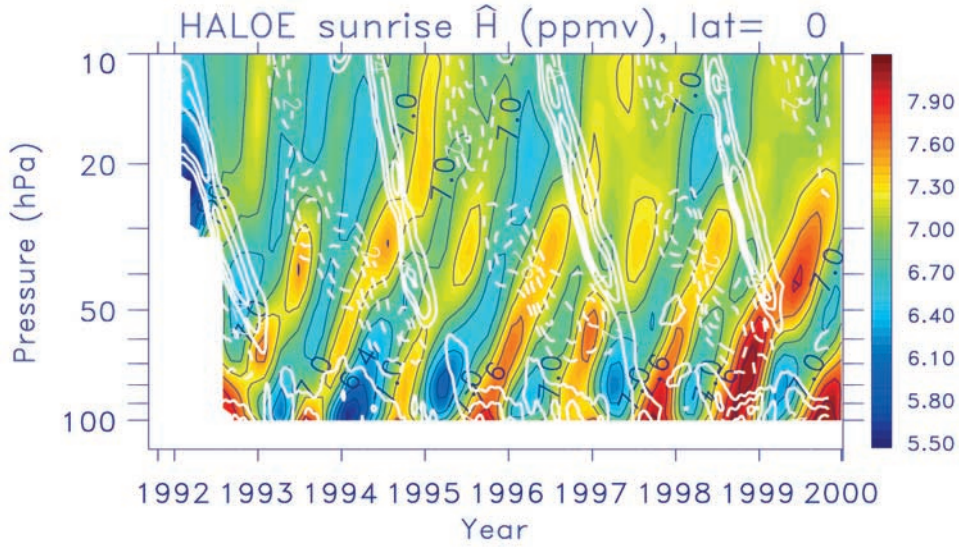

Figure 1. Pressure-time sections of HALOE $\hat{H}$ at the equator (colors and black contours). Vertical shear of zonal wind in Singapore is also plotted (white contours). Contour intervals are 0.3 ppmv for $\hat{H}$, and 2.0 m s^{-1} km^{-1} for vertical shear of zonal wind, with zero contours omitted. Negative values are denoted by dashed contours.

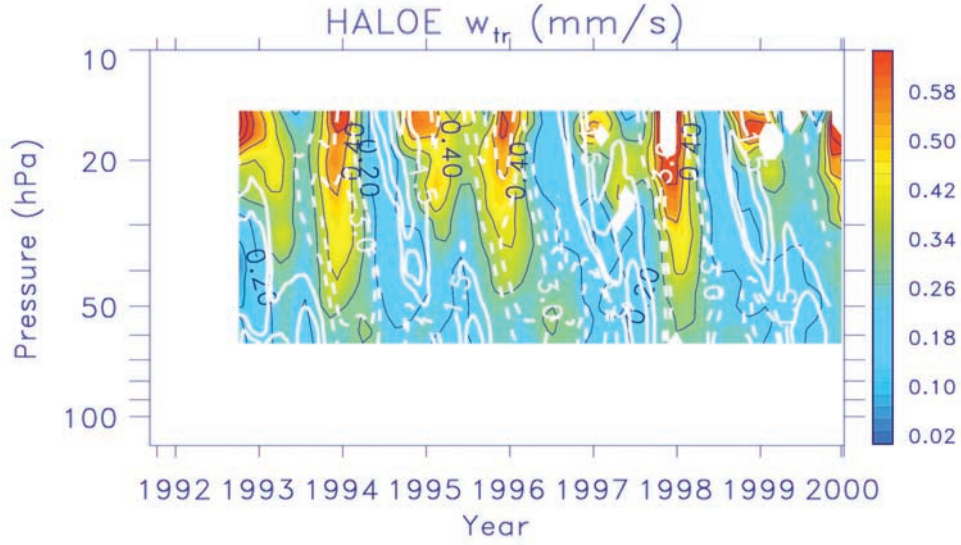

Figure 3. Pressure-time sections of w_{tr} at the equator (colors and black contours). Temperature in Singapore is also plotted at the equator (white contours). Here time mean values of temperature are subtracted from raw values. Contour intervals are 0.1 mm s^{-1} (black) and 1.5 K (white), with zero contours omitted.